Abrupt climate changes during Termination III in Southern Europe

Carlos Pérez-Mejías[a,b,1], Ana Moreno[a], Carlos Sancho[b], Miguel Bartolomé[a,b], Heather Stoll[c,d], Isabel Cacho[e], Hai Cheng[f,g,h], and R. Lawrence Edwards[f]

[a]Department of Geoenvironmental Processes and Global Change, Pyrenean Institute of Ecology–Consejo Superior de Investigaciones Científicas (IPE-CSIC), 50059 Zaragoza, Spain; [b]Earth Sciences Department, University of Zaragoza, 50009 Zaragoza, Spain; [c]Department of Geology, University of Oviedo, 33005 Oviedo, Spain; [d]Department of Earth Sciences, Geological Institute, ETH Zurich, 8092 Zurich, Switzerland; [e]Facultat de Ciències de la Terra, Departament de Dinàmica de la Terra i l'Oceà, Universitat de Barcelona, 08028 Barcelona, Spain; [f]Department of Earth Sciences, University of Minnesota, Minneapolis, MN 55455-0231; [g]Institute of Global Environmental Change, Xian Jiaotong University, Xian 710049, China; and [h]State Key Laboratory of Loess and Quaternary Geology, Institute of Earth Environment, Chinese Academy of Sciences, Xian 710075, China

Edited by Miryam Bar-Matthews, Geological Survey of Israel, Jerusalem, Israel, and accepted by Editorial Board Member Thure E. Cerling August 9, 2017 (received for review December 1, 2016)

The Late Quaternary glacial–interglacial transitions represent the highest amplitude climate changes over the last million years. Unraveling the sequence of events and feedbacks at Termination III (T-III), including potential abrupt climate reversals similar to those of the last Termination, has been particularly challenging due to the scarcity of well-dated records worldwide. Here, we present speleothem data from southern Europe covering the interval from 262.7 to 217.9 kyBP, including the transition from marine isotope stage (MIS) 8 to MIS 7e. High-resolution $\delta^{13}C$, $\delta^{18}O$, and Mg/Ca profiles reveal major millennial-scale changes in aridity manifested in changing water availability and vegetation productivity. uranium–thorium dates provide a solid chronology for two millennial-scale events (S8.1 and S8.2) which, compared with the last two terminations, has some common features with Heinrich 1 and Heinrich 2 in Termination I (T-I).

terminations | stalagmite | stadial event | stable isotopes | Iberian Peninsula

Interpreting the processes responsible for glacial terminations and the accompanying feedbacks requires a detailed chronology across different elements of the climate system. Because of the varying orbital configurations among glacial terminations, it is instructive to compare the sequence of events in different terminations to distinguish common processes and those which are unique. Using records in different parts of the climate system to compare the expression of abrupt climate events at different latitudes may help to diagnose the mechanisms that triggered those transitions. However, it has been difficult to obtain climate records for older terminations, such as Termination III (T-III), with sufficient resolution to capture the abrupt climate events that in some cases result from deglacial meltwater release (1), and to assess which of them are expressed worldwide. In Europe and the Middle East, long lacustrine sequences reveal abrupt changes in sedimentology and vegetation cover over T-III (2–4). Unfortunately, the absence of absolute dates precludes the construction of independent chronologies for these changes and their correlation with marine records of ice volume.

To date, most of the marine and also terrestrial available chronologies of the marine isotope stage (MIS) 8 to MIS 7 transition have been built by either directly or indirectly tuning to orbital configurations (5) or using Antarctic chronologies aligning the benthic $\delta^{18}O$ to deuterium/hydrogen records from Antarctic ice cores (6). Independent chronologies on the marine T-III period, for example in benthic $\delta^{18}O$ records, feature high uncertainty (239 ± 10 ky) (7). Antarctic ice sheet chronologies for T-III based on changes in δD and atmospheric gases have uncertainties estimated at 3–4 ky (8). The absolute chronologies independent of orbital forcing are critical to determine the relationship between paleoclimate records and insolation and to understand ocean-atmosphere feedbacks responsible for deglacial changes. So far, other terrestrial absolute chronologies for T-III are available only in $\delta^{18}O$ records of summer monsoon intensity from Chinese caves (9, 10) and in a $\delta^{18}O$ record of temperature changes from Spannagel Cave in the Alps (11), although this last record starts during early MIS 7e. Here, we present a speleothem geochemical record that covers the full duration of the T-III period in southern Europe, providing a well-dated high-resolution reconstruction of aridity and vegetation productivity which can be related to abrupt stadial events in the North Atlantic caused by glacial meltwater discharges.

The studied speleothem comes from the Ejulve cave (40°45´34´´N 0°35´07´´W, 1,240 m above sea level) (Fig. 1), located in the Iberian Range, NE Spain, under a Mediterranean temperate climate with strong continentality. Results from a 3-y monitoring survey of farmed calcite show that the seasons of positive water balance, autumn through spring, feature low-calcite $\delta^{13}C$ in the precipitated carbonate because soil CO_2 is enhanced by productive vegetation in association with rainy seasons (12) and prior calcite precipitation is minimized. In contrast, high $\delta^{13}C$ occurs during drier periods, and coincides with high Mg/Ca ratios, low amount of in situ farmed calcite, and high temperatures with minima water availability over the cave (*SI Appendix*).

These seasonal oscillations confirm a water availability signal in $\delta^{13}C$ and Mg/Ca ratio; on long time scales changes in the mean temperature during the growth season may also affect vegetation activity and thus $\delta^{13}C$. Therefore, $\delta^{13}C$ record in Ejulve stalagmites is interpreted as a proxy for vegetation productivity

Significance

We present an outstanding speleothem record that reconstructs the vegetation activity and hydrological availability during Termination III (T-III) in Southern Europe throughout $\delta^{13}C$, $\delta^{18}O$, and Mg/Ca variations. The results reveal for the North Atlantic region the sequence of abrupt stadial events during T-III, in close analogy to the Asian Monsoon changes reconstructed from Chinese speleothems. The two stadials identified in this record (S8.1 and S8.2) have similarities with Heinrich 1 and Heinrich 2 events in Termination I in terms of changes in the phasing of benthic $\delta^{18}O$, rise of semidesert pollen taxa, and ice-rafted debris release.

Author contributions: C.P.-M., A.M., C.S., and M.B. designed research; C.P.-M., A.M., C.S., and M.B. performed research; C.P.-M., H.S., I.C., H.C., and R.L.E. contributed new reagents/analytic tools; C.P.-M., A.M., C.S., H.S., and I.C. analyzed data; and C.P.-M., A.M., and C.S. wrote the paper.

The authors declare no conflict of interest.

This article is a PNAS Direct Submission. M.B. is a guest editor invited by the Editorial Board.

[1]To whom correspondence should be addressed. Email: cperez@ipe.csic.es.

This article contains supporting information online at www.pnas.org/lookup/suppl/doi:10.1073/pnas.1619615114/-/DCSupplemental.

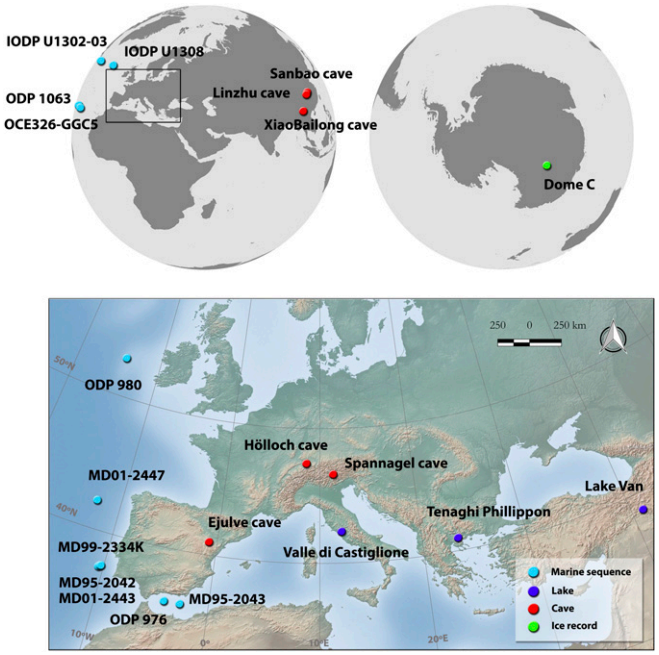

Fig. 1. Location of all records discussed in the text, including the Ejulve cave (this study).

since it is controlled by plant root respiration and microbial activity, and thus conditioned by temperature and especially by humidity. The $\delta^{18}O$ signal in this latitude is complex due to the diverse factors exerting control at the different time scales. Changes in temperature are dominant at the glacial/interglacial time scales while the source of moisture (e.g., freshwater input) has been detected to be important during short events (*SI Appendix*). Calcite precipitates in artificial supports are found throughout the year, but are reduced in summer, a season with water deficit. Thus, a mixing in the isotopic signal of the seasonal values, biased to the higher calcite growth seasons, is expected to be found in fossil speleothems.

Age Model

The 350-mm-long ARTEMISA stalagmite grew from 262.7 to 217.9 kyBP (Fig. 2) with a period of particularly fast growth rate during 240–238 ky, corresponding to the transition from MIS 8 to MIS 7. The chronology is provided by 24 uranium–thorium (U/Th) dates (*SI Appendix*, Table S1), with two reversals (at 45 and 255 mm from the bottom) that were excluded from the age model. From 15 to 65 cm, corresponding to 260–240 ky, U/Th dates fitted by StalAge yield a linear age model and constant slow rates of growth. Dramatically faster growth rates occur over the subsequent 16 cm (70 to 230 mm from base) during MIS 7e. The fast growth rate and absolute age uncertainties of ±2 ky, characteristic of the 1% of uncertainty in age given by the analytical uncertainties propagated through the age equation, complicate a single age interpolation of the entire stalagmite with standard algorithms such as OXCAL software (13) (Fig. 2*A*, orange line) and StalAge (14) (Fig. 2*A*, red line). The final model we use (Fig. 2*B*, green line) is generated using StalAge for the base (seven dates) and top (nine dates) sections of the stalagmite but adding a linear interpolation to connect both parts. This approach provides a more realistic growth post-T-III during earlier MIS 7e and also considers the maximum potential uncertainty given by the U/Th datings (i.e., 2 ky). The fast-growing section permits a resolution of 37 y in the stable isotope record, while the slower-growing glacial and deglacial phases permit 160-y resolution.

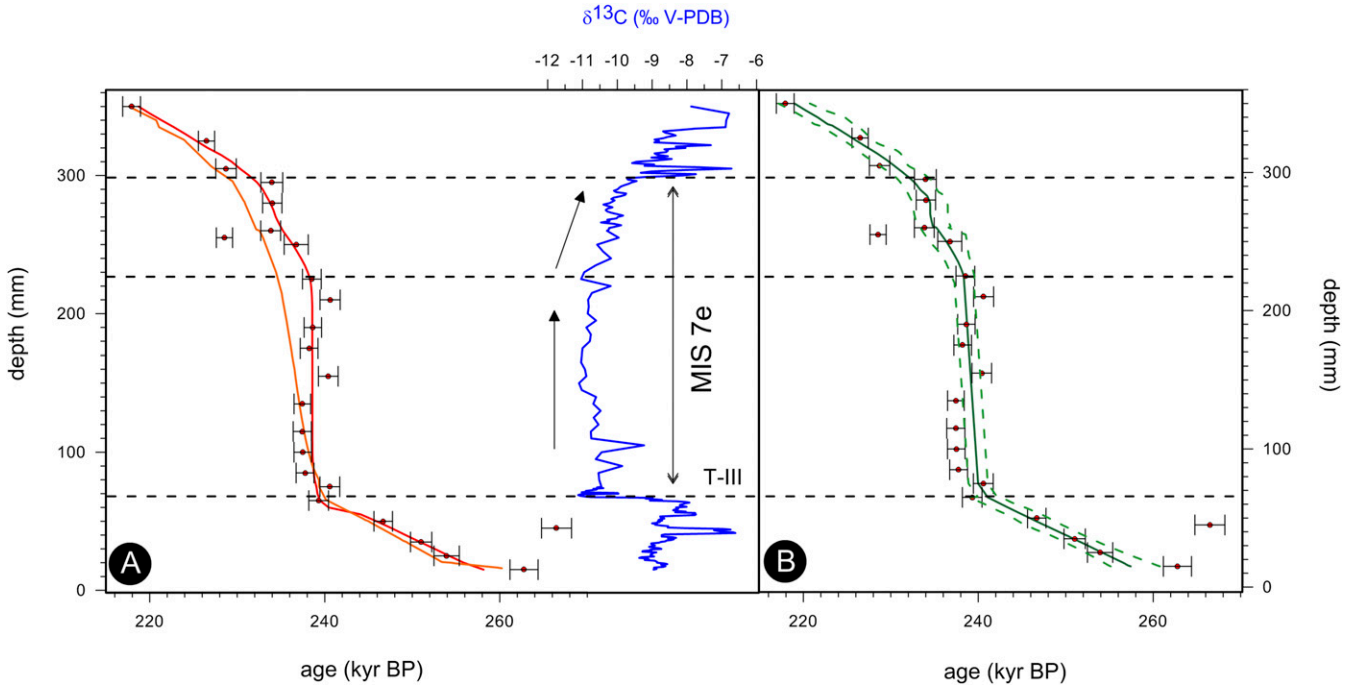

Fig. 2. Age model for ARTEMISA stalagmite. (*A*) Blue line represents $\delta^{13}C$ values to trace the timing of MIS 7e versus depth; red line is the age model constructed by StalAge software (14), and orange line is the model provided by OxCal (13). (*B*) Final model adopted for the stalagmite. Dashed line in the age model represents age uncertainty, provided by StalAge in the top and base parts, and an average dating error used in the lineal interpolation. Horizontal dashed lines establish the glacial–interglacial transitions and the two phases in MIS 7e, according to the changes in growth rate in the age model and the $\delta^{13}C$ profile.

Results and Discussion

Intense isotopic changes in the Ejulve cave speleothem, mostly the change toward more negative $\delta^{13}C$ values, mark the transition from MIS 8 to MIS 7, suggesting a rapid evolution from a generally more arid glacial state with low biological activity to a more humid interglacial with enhanced vegetation productivity (Fig. 3). During this time, the $\delta^{18}O$ values vary from the minimum values of the termination (−9.3‰) at about 243 ky to the maximum in the record (−6.5‰) at 235 ky. The low growth rates during glacial times (3 mm/ky) are consistent with low water availability in the cave during the cold conditions of MIS 8.

Afterward, the onset of MIS 7e is characterized by a rapid $\delta^{13}C$ decrease to −11.1‰, a gradual rise in the $\delta^{18}O$, and a dramatic increase in growth rate to 91 mm/ky (Fig. 3). Following this exceptional increase, growth rates remain higher (20–30 mm/ky) than those of the glacial until 234 ± 2.0 ky before descending to rates near to 6 mm/ky, which are similar to those of MIS 8. This growth rate pattern is consistent with more humid and vegetated interglacial. Likewise, the minima in $\delta^{234}U$ (Fig. 3) between 240 ± 1.1 and 234 ± 2.0 ky compared with previous and following values suggest shorter water residence times in the epikarst during the interglacial (15). The delay of 1 ky in $\delta^{234}U$ with respect to $\delta^{13}C$ and metal ratios at the end of the glacial period indicates a climatic-dependent signal, as seen in other records (15). Two abrupt excursions to more positive $\delta^{13}C$ precede the main deglacial $\delta^{13}C$ depletion from 244.7 ± 2.1 to 241 ± 1.5 and from 249 ± 1.9 to 247.4 ± 2.0 ky [labeled here as Stadial 8.1 and 8.2 events, respectively, identified previously in ice-rafted debris (IRD) layers (16)] which are also marked as transient increases in Mg/Ca and, at least the 8.1 Stadial, as decrease in $\delta^{18}O$ (Fig. 3). Those two events were previously found in Chinese caves (Fig. 3).

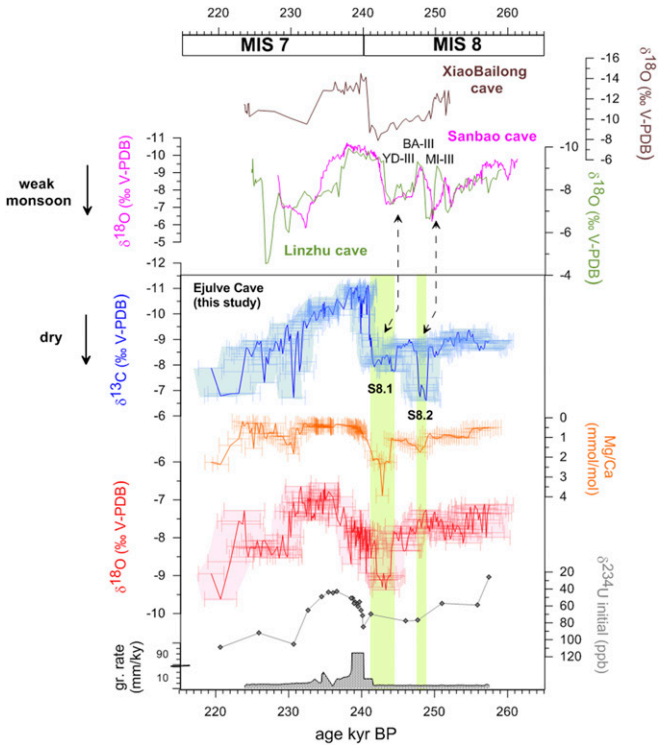

Fig. 3. Results of ARTEMISA stalagmite compared with other records of T-III, from top to bottom: $\delta^{18}O$ profiles from XiaoBailong cave (9) (dark brown), Linzhu cave (10) (light green), and Sanbao cave (10) (pink) [the events YD-III, BA-III, and MI-III identified by Cheng et al. (10) are indicated]. The axes in the Chinese caves are reversed; the results of this study are composed of $\delta^{13}C$ (blue) and $\delta^{18}O$ (red) profiles (the shadow area represents uncertainty range in the chronology) and Mg/Ca (orange) metal ratio (both with axes reversed), $\delta^{234}U$ initial (gray) and growth rate (black and gray). All of the axes are reversed except the growth rate one. Green band indicates dry events, highlighting S8.1 and S8.2, characterized by a trend to higher $\delta^{13}C$ and Mg/Ca values and lower $\delta^{18}O$ in S8.1.

Abrupt Climatic Changes and Forcing Mechanisms During T-III. Glacial terminations appear to be explained not only by rising high latitude or northern Hemisphere insolation (17), but also due to feedbacks from changes in ocean circulation and the carbon cycle (18, 19). When orbital forcing initiates significant melting of a large NH ice sheet, it provides enough meltwater to produce a collapse on the Atlantic Meridional Overturning Circulation (AMOC) (17, 18) which in turn through the bipolar seesaw accelerates Southern Ocean warming and alters wind regimes leading to rapid release of CO_2 from upwelled deep ocean waters to the atmosphere. This greenhouse forcing may be a key impulse making a termination inevitable.

While the conditions for an interglacial onset are conditioned by astronomical pacing (high insolation–low precession), the precise (millennial-scale) timing of each termination and the strength of the following interglacial varies, influenced by key global climate parameters (e.g., ice volume, regional surface temperature, greenhouse gases) (18). The role of such feedbacks and short oscillations has been well characterized for T-I and more recently for Termination II (T-II) (20), but their role in the T-III has not been previously described. The orbital configuration of T-III, with an ∼10-ky lag between maximum in obliquity and minimum in precession (Fig. 4), is very distinctive from that of T-II and T-I (10, 17). T-III is a low-amplitude termination (19) that leads to a weak interglacial, with a rapid return to near full glacial benthic $\delta^{18}O$ within 20 ky after the termination. However, in terms of the sequence of abrupt climate events associated with the termination, T-III has been considered similar to T-I (terminations interrupted by stadials) and different from T-II and Termination IV (T-IV) (uninterrupted or minimally interrupted terminations) according to the study of Chinese stalagmites (10).

The freshwater glacial melt release and AMOC shutdown leave a clear climatic fingerprint on the Iberian Peninsula during stadial events of T-I and MIS 3 because weakened heat transport shifted storm tracks and led to extremely dry conditions (21, 22). This connection results from the expansion of the polar vortex during AMOC shutdowns, which lead to the southward arrival of polar or continental air outbreaks. Several pollen sequences have demonstrated the synchrony of shifts to arid-adapted vegetation in the Iberian Peninsula and the marine cooling (23, 24). A further proof for this tight AMOC–Iberia connection during T-I is provided by an accurately dated speleothem record from the southern Pyrenees which shows parallel changes in humidity and AMOC intensity along the Younger Dryas period (YD) (25).

We propose that the millennial-scale aridity events detected in the Ejulve record at the onset and within the T-III (S8.1 and S8.2 events) are likewise related to AMOC slowdowns or shutdowns. The arid events recorded by high $\delta^{13}C$ and high Mg/Ca in the Ejulve T-III record provide an absolute chronology for the marine record of abrupt changes, where arid events are manifest by the dominance of semidesert pollen in Iberian margin sediments (Fig. 4*J*) and are coincident with enhanced IRD deposition (Fig. 4*I*).

Our T-III record shows a two-phase structure, with a first extreme arid event (S8.2) at 249–247.4 ky, a return to more humid conditions, and a second arid event (S8.1) at 244.7–241 ky (Fig. 4*D*). The imprint of the $\delta^{18}O$ differs between both events and only the S8.1 event is pointed out with extremely low values. The sudden arrival of fresh (^{18}O-depleted) meltwater to North Atlantic intermediate latitudes and entrance in the Mediterranean Sea would provide a mechanism to explain the low $\delta^{18}O$ signal during S8.1 in an analogous way that occurred during T-I

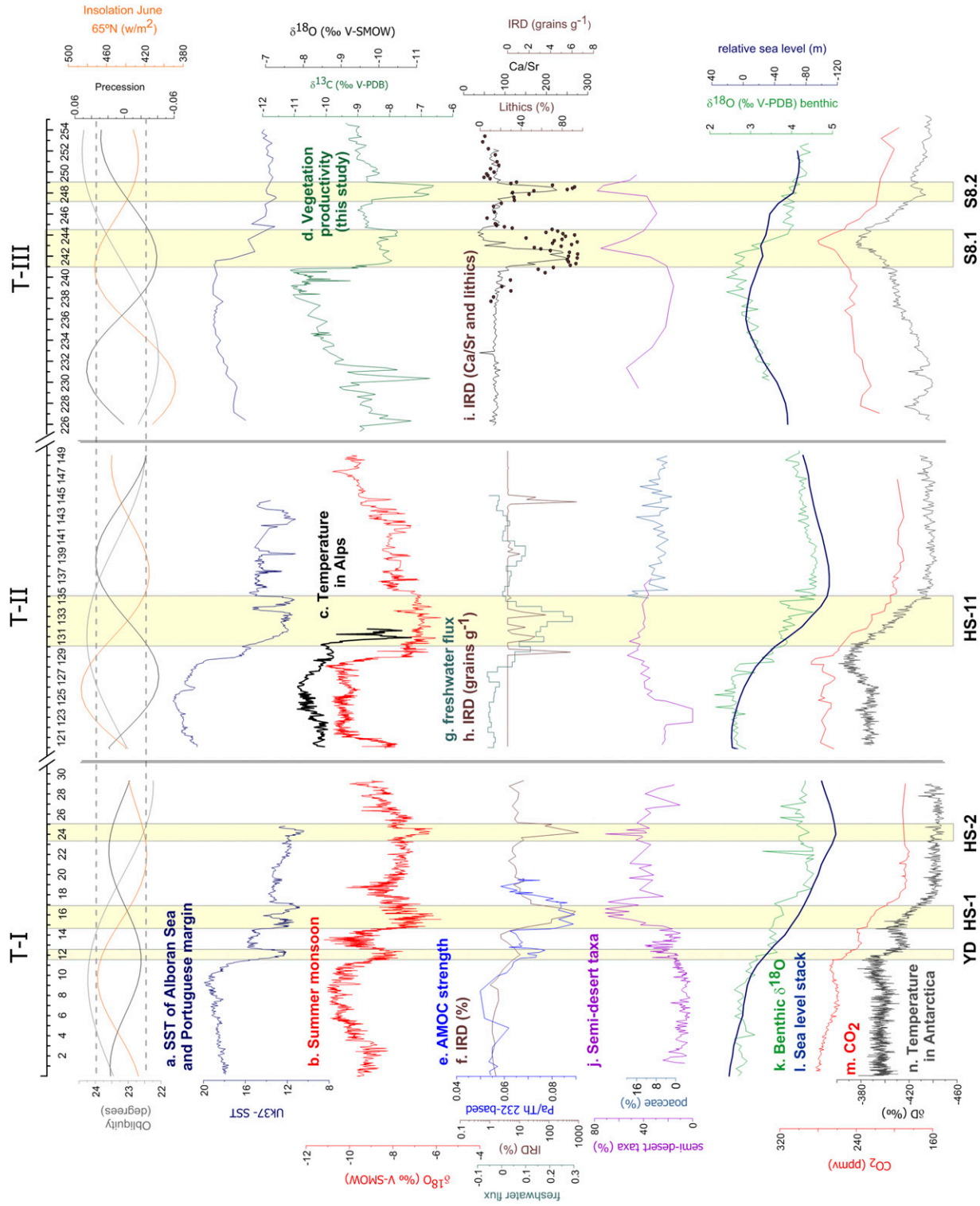

Fig. 4. Comparison of T-I, T-II, and T-III, from top to bottom: orbital forcing including obliquity (gray), precession (black), and insolation curves in June at 65°N (W/m^2) (orange); (*A*) Uk37 SST from marine cores ODP 976 (Alboran Sea) in T-I (1) and T-II (20), and MD01-2443 (Portuguese margin) in T-III (36) (navy blue); (*B*) δ^{18}O composite from Chinese caves as a proxy of summer monsoon intensity (28) (red); (*C*) δ^{18}O profile of Hölloch cave (37) (black); (*D*) δ^{13}C of ARTEMISA from Ejulve Cave (forest green); (*E*) Pa/Th 232-based as AMOC intensity proxy (38) (blue); (*F*) IRD from MD99-2334K (39) (dark brown); (*G*) freshwater flux reconstruction (20) (moss green); (*H*) IRD discharge in ODP-1063 (32) (dark brown); (*I*) Ca/Sr from IODP U1302-03 (16) (black line) and lithics from IODP 1308 (40) (dots, dark brown) in percent; (*J*) semidesert taxa of pollen in MD95-2043 and MD95-2042 (21, 30) in T-I and T-II (purple), poaceae taxa in MD01-2444 (31) (blue), and semidesert taxa of pollen in MD01-2447 (5) in T-III (purple); (*K*) δ^{18}O of benthic foraminifera in IODP U1308 (41) (forest green), (*L*) sea-level stack (42) (deep navy blue); (*M*) CO_2 (ppmv) (43) (red); and (*N*) δD (44) (gray) both in Dome C, Antarctica. Yellow vertical bars represent YD, Heinrich 1, and Heinrich 2 in T-I; Heinrich 11 in T-II; and S8.1 and S8.2 stadials in T-III established in ARTEMISA from the Ejulve cave. Due to the lack of absolute chronologies in the pollen record of T-III, that profile from Iberian Margin has been tuned to the age model of ARTEMISA, using tie points anchored to S8.2, S8.1, and at the end of the MIS 7e. The profile with the original ages can be found in *SI Appendix*, Fig. S7.

(Heinrich 1) and T-II (Heinrich 11) (26). Other records in the Iberian Peninsula have reported a similar isotopic response to the arrival of fresh water to North Atlantic (e.g., during the 8.2-ky event) (27), reinforcing the hypothesis that changes in North Atlantic and Mediterranean sea water may modify rainwater isotopic composition in the Iberian Peninsula and, consequently, $\delta^{18}O$ in speleothems. The shift to low values in $\delta^{18}O$ of ARTEMISA during event S8.1 is very similar to the change reported previously for the Holocene stalagmite [1.7‰ in S8.1 with respect to 2‰ in the 8,200-y event (27)]. On the contrary, $\delta^{18}O$ values do not change during the S8.2 event. That event has more enriched $\delta^{13}C$ values than S8.1, pointing out a lower vegetation activity in our area, in coherence with the record from Chinese caves with weaker monsoon in S8.2 with respect to S8.1 (Fig. 3). A similar structure for the T-III in two phases has already been described in Asian monsoon speleothems (10). Therefore, Ejulve Stadials that are correlated within the dating uncertainty with two similar events of weak summer monsoon in the $\delta^{18}O$ signal from Sanbao Cave (Fig. 3) are the first expression of those abrupt climate changes during T-III in a continental record from Europe.

There are clear teleconnections between the monsoon system and our latitudes, both responding to changes in North Atlantic oceanic conditions that would explain this covariation between records. During the ice-sheet disintegration, the cold anomalies in the ocean generate an influx of meltwater and iceberg discharges in the North Atlantic, triggering the reduction or shutdown of the AMOC and the associated northward surface-ocean transport of heat. The extensive ice cover would seal off the escape of heat to the atmosphere, triggering cold anomalies during winter that probably advected eastward into Asia, affecting the summer monsoon (10, 28). Thus, both Chinese speleothems and our record respond to common mechanisms of climate forcing.

Millennial-Scale Stadial Events in the Context of Last Three Terminations. Taking into account the similar structure established in monsoon records between terminations interrupted by stadials (T-I and T-III) on one hand, and uninterrupted or minimally interrupted terminations (T-II and T-IV) on the other hand, Cheng et al. suggested that in the last four terminations only T-I and T-III show abrupt events in their structure. The possible cause of this different structure among the terminations is associated with the relatively low insolation shifts and rates of insolation change in T-I and T-III, in opposition to the high shifts and rates reported from uninterrupted terminations (T-II and T-IV) (10).

In T-III, whereas the two abrupt weak monsoon events were previously considered analogous to the Mystery Interval and YD (Fig. 3), our direct correlation of the Iberian arid events to the regional marine sequences, the benthic $\delta^{18}O$ record, and the IRD discharges, suggests instead that they are more analogous to the Heinrich 2 (HS-2) and Heinrich 1 (HS-1) in spite of some dissimilarities are also observed (Fig. 4). One of the reasons to make an analogy with Ejulve stadials S8.1 and S8.2 during T-III, with HS-1 and HS-2, lies in their correspondence with two strong IRD events in the North Atlantic Ocean (Fig. 4*I*), which have an intensity similar to those of the MIS 3 (29). In a similar way, HS-1 and HS-2 events preceding the T-I are synchronous with a strong IRD event, while no IRD occurs during the YD (Fig. 4*F*). The AMOC slowdown during the HS-1 (Fig. 4*E*) is coincident with the first appreciable shift in $\delta^{18}O$ of benthic foraminifera (Fig. 4*K*) due to a massive arrival of meltwater to the North Atlantic latitudes and its penetration into the deep ocean. During T-III, the first rise in $\delta^{18}O_{benthic}$ occurs during S8.1 (Fig. 4*K*), indicating the arrival of a large volume of meltwater also coincident with an AMOC slowdown in a similar way to that of T-I, underscoring the similarities between HS-1 and S8.1. However, the arid event and AMOC slowdown of S8.2 were not coincident nor preceded by an appreciable $\delta^{18}O_{benthic}$ change, more analogous to the HS-2, where a small volume of meltwater not appreciable in $\delta^{18}O_{benthic}$ released in particularly sensitive locations was able to accomplish AMOC slowdown. Likewise during T-II, the sea-surface temperatures show during HS-11 (20) a similar structure to HS-1 (Fig. 4*A*), being thus similar to the S8.1 event found in ARTEMISA stalagmite in terms of IRD discharge and arrival of freshwater (Fig. 4 *G* and *H*). On the contrary, arid conditions were not reported from the pollen taxa, albeit it can be due to the scarce pollen records in this area during MIS 6 (30, 31). Moreover, stadial events similar to S8.2 during T-II have not been found in marine sequences, European or Chinese caves (Fig. 4 *A*–*C*). Hence, more data of T-II are needed to confirm or discard the existence of two stadial events or only one in that termination.

Therefore, the similitudes between stadial events S8.1 and S8.2 to HS-1 and HS-2 are defined by the intense IRD discharges, the existence of arid events interpreted from the pulses of dominance of semidesert taxa, and the similar phasing of the benthic $\delta^{18}O$, features not seen during the YD. However, there are also some dissimilarities between S8.1 and HS-1 that should be taken into account and suggest that the analogy between S8.1 and HS-1 is not as strong as between S8.2 and HS-2. Due to the timing of the deglaciation, the relative sea level and the summer insolation differs between S8.1 and HS-1, on which the glacier conditions are more evident. However, the Antarctic warming and the forcing of the CO_2 linked to the AMOC strength (32) differ in the last three terminations (Fig. 4 *M* and *N*). While in T-I the rise in Antarctic temperatures is interrupted by the Bølling–Allerød warm period in the North Hemisphere, conforming a two-peak structure in δD and CO_2, on the contrary T-II and T-III exhibit an uninterrupted rise in Antarctic temperatures following the termination. The AMOC strength is known to be crucial in the development (or not) of a YD-like event in the moment of meltwater discharge due to the deglaciation (33). In that way, the dissimilarities between YD and S8.1 do not rule out definitely the hypothesis of an analog of the YD event in T-III, but are in line with the view of the YD as a very particular abrupt change triggered by complex and multiple processes (34).

Concluding Remarks

The stalagmite ARTEMISA from the Ejulve cave covers the full duration of T-III, which in contrast to T-I and T-II is poorly known due to the scarcity of high precision and well-dated records. This speleothem reconstructs abrupt arid events using $\delta^{13}C$ and Mg/Ca, which have been verified as aridity proxies in the cave by 3 years of cave monitoring. Variation in $\delta^{18}O$ also marks the latest (S8.1) of those two events, indicating a change in the $\delta^{18}O$ composition of the sea water in the source of moisture, probably associated with the entrance of freshwater. Due to the latitudinal and geographical location of the Iberian Peninsula, the sensitivity of this area to AMOC changes during T-I and MIS 3 has been demonstrated. Now, the results of ARTEMISA presented here identify two millennial-scale events (S8.1 and S8.2) that are also related to AMOC slowdowns during MIS 8. The stadial events have some similarities with HS-1 and HS-2, respectively, rather than to YD and HS-1 of the T-I. These similarities, after comparing with T-I and T-II records, are supported by intense IRD discharges, the dominance of semidesert taxa that characterize these event as arid intervals, and the similar phasing of the benthic $\delta^{18}O$. However, changes in sea level and insolation during S8.1 are more similar to YD than HS-1, precluding the identification of the YD as a unique feature of the most recent termination.

Methods

ARTEMISA is a 415-mm-long stalagmite from Ejulve Cave (we work with the first 350 mm from base) collected in situ. No active drip was found over the

stalagmite. The location of the sample inside the cave can be found in *SI Appendix*. The sample was cut with a diamond saw along the growth axis, and polished before sampling. The sample shows a change in the growing edge at 255 mm, probably due to locally hydrological factors. Several thin sections were prepared along the stalagmite, and samples were drilled to U/Th dating, stables isotopes, trace element, and X-ray diffraction (XRD). A total of 236 samples were drilled to stable isotopes with a 0.5-mm microdrill tip in different intervals, 0.5 mm during periods of low growth (from 15 to 75 mm and from 260 to 305 mm from bottom) and 5 mm during faster growth periods (from 75 to 260 mm). The temporal resolution for stables isotopes varies between 37 and 1,406 y, with an average resolution of 194 y. To analyze trace metals, 168 samples were drilled using a 1-mm microdrill tip in equal intervals of 1 mm. In the case of U/Th dating, 24 samples were drilled at different intervals covering the whole stalagmite growth, focusing on identifying potential hiatus or low-growth periods.

Stable isotope analyses were performed at the University of Barcelona (Scientific-Technical Services), and University of Oviedo, using a Finnigan-MAT 252 mass spectrometer fitted with a Kiel Carbonate Device I. Standards were run every 6–10 samples with a reproducibility of 0.02‰ for $\delta^{13}C$ and 0.06‰ for $\delta^{18}O$. Values are reported as $\delta^{18}O$ (‰) and $\delta^{13}C$ (‰) with respect to the Vienna Pee Dee Belemnite standard.

Trace metals analysis was performed in Instituto Pirenaico de Ecologia, Spanish Scientific Research Council (IPE-CSIC) laboratories with an atomic emission spectroscopy (ICP-AES) (Thermo Scientific iCAP DUO 6300) using molar ratios of Mg and Sr in relation to Ca. U/Th datings were analyzed in a multi-collector mass spectrometry (MC-ICP-MS) (Thermo-Finnigan Neptune) at the University of Minnesota following the methodology described in ref. 35. Thin sections were elaborated in University of Zaragoza (rock preparation services). XRD analyses were performed in the Jaume Almera Institute of the CSIC with a Bruker-AXS D5005 powder diffractometer configured in theta-2theta geometry.

ACKNOWLEDGMENTS. This work is a contribution of Geomorfología y Cambio Global and PaleoQ (IUCA) research groups (Aragón Government). We are grateful to Yanbin Lu for helping during the dating process, Ana Méndez for useful advice during stable isotope analysis, Joaquin Perona for the analyses of isotopes on calcite samples, Penélope González-Sampériz for pollen diagram interpretation, and to all the people who helped during field work and sampling in the IPE-CSIC laboratory. We acknowledge a Government of Aragón predoctoral research grant and the CTM2013-48639-C2-2-R (OPERA) and CGL2016-77479-R (SPYRIT) projects for funding, and partial support from NSF AGS 1702816 to R.L.E. and H.C. We thank the editor and two anonymous reviewers for detailed comments and constructive criticism, which resulted in improvements to the paper.

1. Martrat B, Jimenez-Amat P, Zahn R, Grimalt JO (2014) Similarities and dissimilarities between the last two deglaciations and interglaciations in the North Atlantic region. *Quat Sci Rev* 99:122–134.
2. Tzedakis C (2005) Towards an understanding of the response of southern European vegetation to orbital and suborbital climate variability. *Quat Sci Rev* 24:1585–1599.
3. Kwiecien O, et al. (2014) Dynamics of the last four glacial terminations recorded in Lake Van, Turkey. *Quat Sci Rev* 104:42–52.
4. Tzedakis PC, et al. (1997) Comparison of terrestrial and marine records of changing climate of the last 500,000 years. *Earth Planet Sci Lett* 150:171–176.
5. Desprat S, et al. (2006) Climatic variability of Marine Isotope Stage 7: Direct land–sea–ice correlation from a multiproxy analysis of a north-western Iberian margin deep-sea core. *Quat Sci Rev* 25:1010–1026.
6. Tzedakis PC, Roucoux KH, de Abreu L, Shackleton NJ (2004) The duration of forest stages in southern Europe and interglacial climate variability. *Science* 306:2231–2235.
7. Huybers P, Wunsch C (2005) Obliquity pacing of the late Pleistocene glacial terminations. *Nature* 434:491–494.
8. Bazin L, et al. (2013) An optimized multi-proxy, multi-site Antarctic ice and gas orbital chronology (AICC2012). *Clim Past* 9:1715–1731.
9. Cai Y, et al. (2015) Variability of stalagmite-inferred Indian monsoon precipitation over the past 252,000 y. *Proc Natl Acad Sci USA* 112:2954–2959.
10. Cheng H, et al. (2009) Ice age terminations. *Science* 326:248–252.
11. Spotl C, Scholz D, Mangini A (2008) A terrestrial U/Th-dated stable isotope record of the Penultimate Interglacial. *Earth Planet Sci Lett* 276:283–292.
12. Camarero JJ, Gazol A, Tardif JC, Conciatori F (2015) Attributing forest responses to global-change drivers: Limited evidence of a CO_2 -fertilization effect in Iberian pine growth. *J Biogeogr* 42:2220–2233.
13. Ramsey CB (2008) Deposition models for chronological records. *Quat Sci Rev* 27:42–60.
14. Scholz D, Hoffmann DL (2011) StalAge - An algorithm designed for construction of speleothem age models. *Quat Geochronol* 6:369–382.
15. Hellstrom J, McCulloch M (2000) Multi-proxy constraints on the climatic significance of trace element records from a New Zealand speleothem. *Earth Planet Sci Lett* 179: 287–297.
16. Channell JET, et al. (2012) A 750-kyr detrital-layer stratigraphy for the North Atlantic (IODP Sites U1302–U1303, Orphan Knoll, Labrador Sea). *Earth Planet Sci Lett* 317–318: 218–230.
17. Denton GH, et al. (2010) The last glacial termination. *Science* 328:1652–1656.
18. Past Interglacials Working Group of PAGES (2016) Interglacials of the last 800,000 years: Interglacials of the last 800,000 years. *Rev Geophys* 54:162–219.
19. Lang N, Wolff EW (2011) Interglacial and glacial variability from the last 800 ka in marine, ice and terrestrial archives. *Clim Past* 7:361–380.
20. Marino G, et al. (2015) Bipolar seesaw control on last interglacial sea level. *Nature* 522:197–201.
21. Fletcher WJ, Sánchez Goñi MF (2008) Orbital- and sub-orbital-scale climate impacts on vegetation of the western Mediterranean basin over the last 48,000 yr. *Quat Res* 70: 451–464.
22. Moreno A, et al. (2005) Links between marine and atmospheric processes oscillating at millennial time-scale. A multy-proxy study of the last 50,000 yr from the Alboran Sea (Western Mediterranean Sea). *Quat Sci Rev* 24:1623–1636.
23. Goñi MS, et al. (2002) Synchroneity between marine and terrestrial responses to millennial scale climatic variability during the last glacial period in the Mediterranean region. *Clim Dyn* 19:95–105.
24. González-Sampériz P, et al. (2006) Climate variability in the Spanish Pyrenees during the last 30,000 yr revealed by the El Portalet sequence. *Quat Res* 66:38–52.
25. Bartolomé M, et al. (2015) Hydrological change in Southern Europe responding to increasing North Atlantic overturning during Greenland Stadial 1. *Proc Natl Acad Sci USA* 112:6568–6572.
26. Jiménez-Amat P, Zahn R (2015) Offset timing of climate oscillations during the last two glacial-interglacial transitions connected with large-scale freshwater perturbation. *Paleoceanography* 30:768–788.
27. Domínguez-Villar D, et al. (2009) Oxygen isotope precipitation anomaly in the North Atlantic region during the 8.2 ka event. *Geology* 37:1095–1098.
28. Cheng H, et al. (2016) The Asian monsoon over the past 640,000 years and ice age terminations. *Nature* 534:640–646.
29. Birner B, Hodell DA, Tzedakis PC, Skinner LC (2016) Similar millennial climate variability on the Iberian margin during two early Pleistocene glacials and MIS 3. *Paleoceanography* 31:203–217.
30. Goñi MS, Eynaud F, Turon JL, Shackleton NJ (1999) High resolution palynological record off the Iberian margin: Direct land-sea correlation for the Last Interglacial complex. *Earth Planet Sci Lett* 171:123–137.
31. Margari V, et al. (2014) Land-ocean changes on orbital and millennial time scales and the penultimate glaciation. *Geology* 42:183–186.
32. Deaney EL, Barker S, van de Flierdt T (2017) Timing and nature of AMOC recovery across Termination 2 and magnitude of deglacial CO2 change. *Nat Commun* 8:14595.
33. Carlson AE (2008) Why there was not a Younger Dryas-like event during the Penultimate Deglaciation. *Quat Sci Rev* 27:882–887.
34. Renssen H, et al. (2015) Multiple causes of the Younger Dryas cold period. *Nat Geosci* 8:946–949.
35. Cheng H, et al. (2013) Improvements in 230Th dating, 230Th and 234U half-life values, and U–Th isotopic measurements by multi-collector inductively coupled plasma mass spectrometry. *Earth Planet Sci Lett* 371–372:82–91.
36. Martrat B, et al. (2007) Four climate cycles of recurring deep and surface water destabilizations on the Iberian margin. *Science* 317:502–507.
37. Moseley GE, et al. (2015) Termination-II interstadial/stadial climate change recorded in two stalagmites from the north European Alps. *Quat Sci Rev* 127:229–239.
38. McManus JF, Francois R, Gherardi JM, Keigwin LD, Brown-Leger S (2004) Collapse and rapid resumption of Atlantic meridional circulation linked to deglacial climate changes. *Nature* 428:834–837.
39. Skinner L, Shackleton N (2004) Rapid transient changes in northeast Atlantic deep water ventilation age across Termination 1. *Paleoceanography* 19:PA2005.
40. Obrochta SP, et al. (2014) Climate variability and ice-sheet dynamics during the last three glaciations. *Earth Planet Sci Lett* 406:198–212.
41. Hodell DA, Channell JET, Curtis JH, Romero OE, Röhl U (2008) Onset of "Hudson Strait" Heinrich events in the eastern North Atlantic at the end of the middle Pleistocene transition (~640 ka)? *Paleoceanography* 23:PA4218.
42. Spratt RM, Lisiecki LE (2016) A Late Pleistocene sea level stack. *Clim Past* 12:1079–1092.
43. Lüthi D, et al. (2008) High-resolution carbon dioxide concentration record 650,000-800,000 years before present. *Nature* 453:379–382.
44. Jouzel J, et al. (2007) Orbital and millennial Antarctic climate variability over the past 800,000 years. *Science* 317:793–796.